Draft version May 17, 2024
Typeset using LaTeX default style in AASTeX631

Anomalous radial acceleration of galaxies and clusters supports hyperconical modified gravity

Robert Monjo [1] and Indranil Banik [2]

[1] Department of Algebra, Geometry and Topology, Complutense University of Madrid
Pza. Ciencias 3, E-28040 Madrid, Spain, rmonjo@ucm.es
[2] Scottish Universities Physics Alliance, University of Saint Andrews, North Haugh, Saint Andrews, Fife, KY16 9SS, UK

Submitted to ApJ

ABSTRACT

General relativity (GR) is the most successful theory of gravity, with great observational support at local scales. However, to keep GR valid at over cosmic scales, some phenomena (such as the flat galaxy rotation curves and the cosmic acceleration) require the assumption of exotic dark matter. The radial acceleration relation (RAR) indicates a tight correlation between dynamical mass and baryonic mass in galaxies. This suggests that the observations could be better explained by modified gravity theories without exotic matter. Modified Newtonian Dynamics (MOND) is an alternative theory that was originally designed to explain flat galaxy rotation curves by using a new fundamental constant acceleration a_0, the so-called Milgromian parameter. However, this non-relativistic model is too rigid (with insufficient parameters) to fit the large diversity of observational phenomena. In contrast, a relativistic MOND-like gravity naturally emerges from the hyperconical model, which derives a fictitious acceleration compatible with observations. This study analyses the compatibility of the hyperconical model with respect to RAR observations of 10 galaxy clusters obtained from HIFLUGCS and 60 high-quality SPARC galaxy rotation curves. The results show that a general relation can be fitted to most cases with only one or two parameters, with an acceptable chi-square and p-value. These findings suggest a possible way to complete the proposed modification of GR on a cosmic scale.

1. INTRODUCTION

1.1. *The dark matter missing gravity problem*

As is well known, observational tests of General Relativity (GR) show successful results on Solar System scales (Dittus & Lämmerzahl 2007; Ciufolini et al. 2019; Touboul et al. 2022; Liu et al. 2022; Desmond et al. 2024; Vokrouhlický et al. 2024). The good skill of standard gravity seems to be in question only on larger scales (Chae et al. 2020; Banik & Zhao 2022). It is well-known that exotic cold dark matter (CDM) is required to extend GR to cosmic scales. However, the not-yet-discovered CDM particles present strong theoretical challenges, such as explaining the tight empirical relationship between observed gravitational anomalies (assimilated to CDM) and the distribution of visible baryonic matter in galaxies (Trippe 2014; Merritt 2017; Goddy et al. 2023). This empirical law is known as the mass-discrepancy acceleration relation (MDAR, McGaugh 2004; Di Cintio & Lelli 2015; Desmond 2016), the mass-luminosity relation (Leauthaud et al. 2010; Cattaneo et al. 2014), the baryonic Tully-Fisher relation (BTFR, Lelli et al. 2019; Goddy et al. 2023), or the more general radial acceleration relation (RAR; McGaugh et al. 2016; Lelli et al. 2017; Tian et al. 2020).

Tian et al. (2020) found that the observed RAR in galaxy clusters is consistent with predictions from a semi-analytical model developed in the standard Lambda-CDM (ΛCDM) framework. To explain how the contribution of CDM is determined by that of baryons, some authors suggest that they present a strong coupling that leads to an effective law such as the MDAR/BTFR/RAR (Blanchet 2007; Katz et al. 2016; Barkana 2018).

However, the lack of direct detection (or indirect non-gravitational) of dark matter suggests a weak or even non-existent coupling between CDM and baryons (Abel et al. 2017; Hoof et al. 2020; Du et al. 2022; Aalbers et al. 2023; Hu et al. 2024), which is in conflict with these empirical relationships. Moreover, excess rotation occurs only where the Newtonian acceleration a_N induced by the visible matter is lower than a typical scale of about $a_N \lesssim a_0 \approx 1.2\times10^{-10}\mathrm{m\,s^{-2}}$, suggesting that it is a space-time problem rather than a matter-type problem. This is also consistent

with the deficient dark-matter halos that some relic galaxies (above of the a_0 scale) seem to indicate (Comerón et al. 2023). In other cases, the CDM halo hypothesis also predicts a systematically deviating relation from the observations, with densities about half of what is predicted by CDM simulations (de Blok et al. 2008), while the rotation curves appear to be more naturally explained by modified gravity (McGaugh et al. 2007, 2016; Famaey & McGaugh 2012; Banik & Zhao 2022; Chae 2022).

The hypothesis of 'dark matter' also presents difficulties in explaining some phenomena such as the absence of the expected *Chandrasekhar dynamical friction* in cluster collisions, falsified by more than 7 sigmas (Kroupa 2015; Ardi & Baumgardt 2020; Kroupa et al. 2023). The lack of dynamical friction on galaxy bars is a strong argument that the central density of CDM in typical disc galaxies has to be a lot smaller than expected in standard CDM simulations (Roshan et al. 2021). Another example is the morphology of dwarf galaxies. According to Asencio et al. (2022), observed deformations of dwarf galaxies in the Fornax Cluster and the lack of low-surface-brightness dwarfs toward its center are incompatible with ΛCDM predictions. Moreover, the dwarfs analyzed in that study have sufficiently little stellar mass that the observations cannot be explained by baryonic feedback effects, but they are consistent with the Milgromian modified Newtonian dynamics (MOND; Milgrom 1983). Therefore, most observations suggest the need to explore modified gravity as an alternative to the standard model (Trippe 2014; Merritt 2017).

1.2. *Beyond the MOND paradigm*

The MOND paradigm has been deeply explored, from galactic dynamics to the *Hubble tension*, which is explained by a more efficient (early) formation of large structures such as the local supervoid (Keenan et al. 2013; Haslbauer et al. 2020; Banik & Zhao 2022; Mazurenko et al. 2023). In fact, RAR has been thoroughly analyzed for galaxy rotation curves collected from the Spitzer Photometry and Accurate Rotation Curves (SPARC) sample (Lelli et al. 2016, 2019). The results were anticipated over three decades ago by MOND (Milgrom 1983; McGaugh et al. 2016), although the form of the transition between the Newtonian and Milgromian regimes must be found empirically.

However, the relativistic formulation of MOND was less successful. In particular, Bekenstein proposed a non-cosmological version of Tensor-Vector-Scalar (TeVeS) gravity (Bekenstein 2004; Famaey & McGaugh 2012) that predicts unstable stars on a scale of a few weeks (Seifert 2007), which is only avoidable with an undetermined number of terms (Mavromatos et al. 2009). To solve these issues, Skordis & Złośnik (2021) found that, by adding terms analogous to the FLRW action, at least the second-order expansion is free of ghost instabilities. Their model is also capable of obtaining gravitational waves traveling at the speed of light c, which was not the case with the original TeVeS. However, the authors pointed out that it needs to be embedded in a more fundamental theory.

Recently, Blanchet & Skordis (2024) proposed a relativistic MOND formulation based on space-time foliation by three-dimensional space-like hypersurfaces labeled by the Khronon scalar field. The idea is very similar to the Arnowitt–Deser–Misner (ADM) treatment in the dynamical embedding of the hyperconical universe (Monjo 2017, 2018; Monjo & Campoamor-Stursberg 2020; Monjo 2023, 2024a,b).

Applying perturbation theory to the hyperconical metric, a relativistic theory with MOND phenomenology is obtained, which fits adequately to 123 SPARC galaxy rotation curves (Monjo 2023). The cosmic acceleration derived from it is $a_{\gamma 0} := 2\gamma_0^{-1}c/t$, where t is the age of the universe, c is the speed of light, and $\gamma_0 > 1$ is a projection parameter that translates from the ambient spacetime to the embedded manifold (Monjo & Campoamor-Stursberg 2023; Monjo 2024a). In contrast to the Milgrom constant a_0, the cosmic acceleration $a_{\gamma 0}$ is a variable that depends on the geometry considered (mainly the ratio between escape speed and Hubble flux). The equivalence between the a_0 and $a_{\gamma 0}$ scales is found for $\gamma_0 \approx 13 \pm 3$.

In the limit of weak gravitational fields and low velocities, the hyperconical model is also linked to the scalar tensor vector gravity (STVG) theory, popularly known as Moffat's modified gravity (MOG). The MOG/STVG model is a fully covariant Lorentz invariant theory that includes a dynamical massive vector field and scalar fields to modify GR with a dynamical 'gravitational constant' G (Moffat & Toth 2009, 2013; Harikumar & Biesiada 2022). In particular, it leads to an anomalous acceleration of about $2\,G\alpha_G D^2 \approx 1.1\times10^{-10}\mathrm{m\,s^{-2}} \approx 2\gamma_0^{-1}c/t$ for $\gamma_0 \approx 12$, with $\alpha_G \approx 10$ and the universal MOG constant $D = 6.25\times10^3 M_\odot^{1/2}\ \mathrm{kpc}^{-1}$. Fixing these parameters by using galaxy rotation curves, MOG fails to account for the observed velocity dispersion profile of Dragonfly 44 at 5.5 sigma confidence even if one allows plausible variations to its star formation history and thus stellar mass-to-light ratio:

The number of parameters needed to accommodate most theories to the observations of galaxy clusters is perhaps too large and unnatural. In all cases, the phenomenological parameters (e.g., the CDM distribution profile, the ad-hoc MOND interpolating function μ, and the MOG constant D) need additional theoretical motivation. In contrast, the

hyperconical model proposed by Monjo derives a natural modification of GR from minimal dynamical embedding in a (flat) five-dimensional Minkowskian spacetime (Monjo 2023, 2024a,b).

Therefore, this paper aims to show how the anomalous RAR of ten galaxy clusters, analyzed by Eckert et al. (2022) and Li et al. (2023), are adequately modeled by the hyperconical modified gravity (HMG) of Monjo (2023). As Tian et al. (2020) pointed out, clusters present a larger anomalous acceleration ($g \sim 10^{-9}\mathrm{m\,s^{-2}}$) than galaxy rotation curves ($g \sim 10^{-10}\mathrm{m\,s^{-2}}$), reflecting the missing baryon problem that remains a challenge for MOND in galaxy clusters (Famaey & McGaugh 2012; Li et al. 2023; Tian et al. 2024). This open issue is addressed here with the following structure: Sect. 2 summarizes the data used and the HMG model; Sect. 3 shows the main results in the fits and discusses predictions for galaxies and smaller systems, and finally Sect. 4 points out the most important findings and concluding remarks.

2. DATA AND MODEL

2.1. *Observations used*

This study uses observational estimates of the radial acceleration relations (RAR; total gravity observed compared to Newtonian gravity due to baryons) for 10 galaxy clusters ($0.0328 < z < 0.0899$) that were collected from the HIghest X-ray FLUx Galaxy Cluster Sample (HIFLUGCS, Li et al. 2023). In particular, the galaxy clusters considered are as follows: A0085, A1795, A2029, A2142, A3158, A0262, A2589, A3571, A0576, A0496. Moreover, to compare our results, rotation curves were collected from 60 high-quality SPARC galaxies filtered to well-measured intermediate radii (McGaugh et al. 2007, 2016; Lelli et al. 2019).

2.2. *Radial acceleration from hyperconical modified gravity (HMG)*

Observations were used to assess whether the empirical RAR is in agreement with HMG as developed by Monjo (2023) and summarized here. Let g be the background metric of the so-called hyperconical universe (Monjo 2017, 2018; Monjo & Campoamor-Stursberg 2020, 2023). The metric g is locally approximately given by

$$g \approx dt^2\left(1-kr'^2\right) - \frac{t^2}{t_0^2}\left(\frac{dr'^2}{1-kr'^2} + r'^2 d\Sigma^2\right) - \frac{2r't}{t_0^2}\frac{dr'dt}{\sqrt{1-kr'^2}}\,, \tag{1}$$

where $k = 1/t_0^2$ is the spatial curvature for the current value $t_0 \equiv 1$ of the age t of the universe, while t/t_0 is a linear scale factor (Monjo 2024a), $r' \ll t_0$ is the comoving distance, and Σ represents the angular coordinates. The shift and lapse terms of Eq. 1 lead to an apparent radial spatial inhomogeneity that is assimilated as a fictitious acceleration with adequate stereographic projection coordinates, which is a candidate to explain the Hubble tension (Monjo & Campoamor-Stursberg 2023).

On the other hand, any gravitational system of mass M_{sys} generates a perturbation over the background metric $g \to \hat{g}$ (Eq. 1) such that $kr'^2 \to \hat{k}\hat{r}'^2 := k\hat{r}'^2 + 2GM_{sys}/\hat{r}'$. Applying local validity of GR (Appendix A), the perturbation term $\hat{h} := \hat{g} - g$ is a key of the model (Appendix B). Another key is the stereographic projection of the coordinates $r' \to \hat{r}' = \lambda^{1/2} r'$ and $t \to \hat{t} = \lambda t$, given by a scaling factor $\lambda := 1/(1-\gamma/\gamma_0)$ that is a function of the angular position $\gamma = \sin^{-1}(r'/t_0)$ and a projection factor $\gamma_0^{-1} = \gamma_{sys}^{-1}\cos\gamma_{sys}$, where γ_{sys} is the characteristic angle of the gravitational system (Appendix C). In an empty universe, $\gamma_0 = \gamma_U/\cos\gamma_U$. We expect $\gamma_U = \frac{1}{3}\pi$ and therefore that $\gamma_0 = \frac{2}{3}\pi \approx 2$; while the projective factor of maximum causality, $\gamma_0^{-1} = 1$, arises for $\gamma_U \approx 0.235\pi$ as then $\gamma_U = \cos\gamma_U$.

When geodesic equations are applied to the projected time component of the perturbation $\hat{h}_{tt}$, a fictitious cosmic acceleration of roughly $\gamma_0^{-1}c/t$ emerges in the spatial direction (see Appendix C.3):

$$\frac{|a_{Tot} - a_N|}{c/t} \approx \frac{1}{\gamma_0} \approx \frac{\cos\gamma_{sys}}{\gamma_{sys}}\,, \tag{2}$$

where $a_N := GM_{sys}/r^2$ is the Newtonian acceleration. However, a time-like component is also found in the acceleration that contributes to the total centrifugal acceleration a_C such that $a_C \approx \sqrt{a_N^2 + 2c/(\gamma_0 t)}$, which is useful to model galaxy rotation curves under the HMG framework (Monjo 2023). Alternatively to Eq. 2, the cluster RAR is usually expressed as a quotient between total and Newtonian acceleration. That is,

$$\frac{a_{Tot}}{a_N} \approx 1 - \frac{c}{a_N\gamma_0 t}\,, \tag{3}$$

with factor $\gamma_0^{-1} = \gamma_{sys}^{-1} \cos\gamma_{sys}$, where the projective angle γ_{sys} can be estimated from the galaxy cluster approach (Eq. C17) or from the general model (Eq. C15), respectively, by considering the relative geometry (angle) between the Hubble speed $v_H := r/t$ and the Newtonian circular speed $v_C := \sqrt{GM_{sys}/r}$ or its classical escape velocity $v_E := \sqrt{2}\, v_C$, as follows:

$$\sin^2\gamma_{cluster}(r) \approx \sin^2\gamma_{galaxy} - \left(\sin^2\gamma_{galaxy} - \sin^2\gamma_U\right) \frac{v_E^2(r)}{\varepsilon_H^2 v_H^2(r) + v_E^2(r)} \,, \tag{4}$$

$$\sin^2\gamma_{cluster}(r) \approx \sin^2\gamma_U + \left(\sin^2\gamma_{center} - \sin^2\gamma_U\right) \left|\frac{v_E^2(r) - \epsilon_H^2 v_H^2(r)}{v_E^2(r) + \epsilon_H^2 v_H^2(r)}\right| , \tag{5}$$

where the parameter ϵ_H^2 is the so-called *relative density of the neighborhood* (Appendix C.1), while $\gamma_{center} = \pi/2$ and $\gamma_U = \pi/3$ or $\gamma_U \approx 0.235\pi$ can be fixed here to set a 1-parameter (ϵ_H) general model from Eq. 5. As a second-order approach, this study also assumes that $\{\epsilon_H, \gamma_{galaxy}\}$ can be free in our 2-parameter model for clusters (Eq. 4).

3. RESULTS AND DISCUSSION

3.1. *Fitted values*

Individually, fitting of Eq. 4 for the quotient between total and Newtonian acceleration (Eq. 3) leads to a square root of the relative density of about $\varepsilon_H = 38^{+29}_{-11}$ (90% confidence level; Appendix C.4, Fig. C.2). Using the specific model for the clusters (Eq. 4), all fits provide an acceptable χ^2 (p-value < 0.667) except for the A2029 cluster, which did not pass the χ^2 test for the fixed *neighborhood projective angle* of $\gamma_0 = 2$ (i.e., $\gamma_U = \pi/3$). However, it did for $\gamma_0 = 1$ (i.e., $\gamma_U \approx 0.235\pi$), which implies to use the causality limit for the cosmic acceleration instead of the empty-space limit.

Globally, the correlation of RAR values (differences) with respect to the escape-Hubble approach (Eqs. 2 and 4) is slightly higher ($R^2 = 0.83$) than with respect to the Newtonian acceleration ($R^2 = 0.79$). The simplest model of fixing $\gamma_U = \pi/3$ and using a single global parameter, $\varepsilon_H = 40^{+8}_{-6}$, gives a Pearson coefficient of $R^2 = 0.75$, while if $\gamma_U = \pi/3$ is replaced by $\gamma_U = 0.235\pi$, we get instead $R^2 = 0.83$ with $\varepsilon_H = 60^{+20}_{-8}$ (90% confidence level).

Larger anomalies in acceleration are found for the higher escape speeds ($v_E/v_H \sim \varepsilon_H$) in clusters. However, this is the opposite for galaxies, which experience the maximum anomaly for low escape velocities ($v_E/v_H < \varepsilon_H$), as shown in Fig. 1. In clusters, the relative density between the dominant galaxy (BCG) and the neighborhood determines this opposite behavior. The value of $v_E/v_H \sim \varepsilon_H$ points to the transition regime between small and large anomalies.

3.2. *Predictions for galaxy dynamics*

As discussed in Sect. 1, HMG derives a relationship between the Milgrom acceleration $a_0 \approx 1.2\times10^{-10}\mathrm{m/s^2}$ and the cosmic parameter $c/t \approx 6.9\times10^{-10}\mathrm{m/s^2}$, since $a_0 \approx a_{\gamma 0} := 2\gamma_0^{-1} c/t$ for galaxy rotation curves, for an approximately constant $\gamma_0^{-1} \approx 0.08$ (Monjo 2023). However, the geometry of gravitational systems led to a variable value of the projection factor $\gamma_0^{-1} \in (0, 1)$, depending on the ration between escape speed and Hubble flux.

According to the general model of projective angles (Eq. 5), it is expected that galaxies and galaxy clusters exhibit opposite behaviors, but following the same theoretical curve. Using $\gamma_{center} = \pi/2$, $\gamma_U = \pi/3$, and $\varepsilon_H = 56^{+22}_{-12}$ (obtained from the cluster data), we apply Eqs. 2 and 5 to predict the behavior of 60 galaxies, whose data were collected by McGaugh et al. (2007). By directly applying Eq. 5 to the escape speed of galaxies, a relative anomaly of $(a_{Tot} - a_N)/(c/t) = \gamma_0^{-1}$ between 0.05 and 0.40 is predicted, close to the observations of $\gamma_0^{-1} = 0.07^{+0.03}_{-0.02}$ in the galaxy rotation curves.

The wide range of γ_0^{-1} in the clusters depends on the ratio v_e/v_H between the escape speed (v_e) and the Hubble flux (v_H) as well as the central projective angle $0.47\pi \lesssim \gamma_{center} \lesssim 0.50\pi$ and the parameter $\varepsilon_H \geq 1$. For galaxy rotation curves, this additional dependency is not evident beyond the usual dependence on a_N, according to deep reviews of MOND interpolating functions, showing that γ_0 is almost constant and the actual gravity only depends on the Newtonian acceleration (Banik & Zhao 2022; Stiskalek & Desmond 2023). This apparent weakness of the model is easily solved by the fact that an almost constant γ_0^{-1} is obtained from the 2-parameter model (Eq. 5) with fitting γ_{center} (Fig. 2 *top left*). Moreover, the relation of the rotation curves with v_e/v_H is highly nonlinear, since it is within trigonometric functions. Finally, the correlation between Newtonian acceleration $a_N \propto r^{-2}$ and the flux ratio $v_e/v_H \propto r^{-3/2}$ is very high for galaxies ($R \approx 0.90$, p-value < 0.001), so the families of interpolating function $f(a_N)$ remove almost all this nonlinear dependency. In any case, the effective interpolating function of the HMG model is

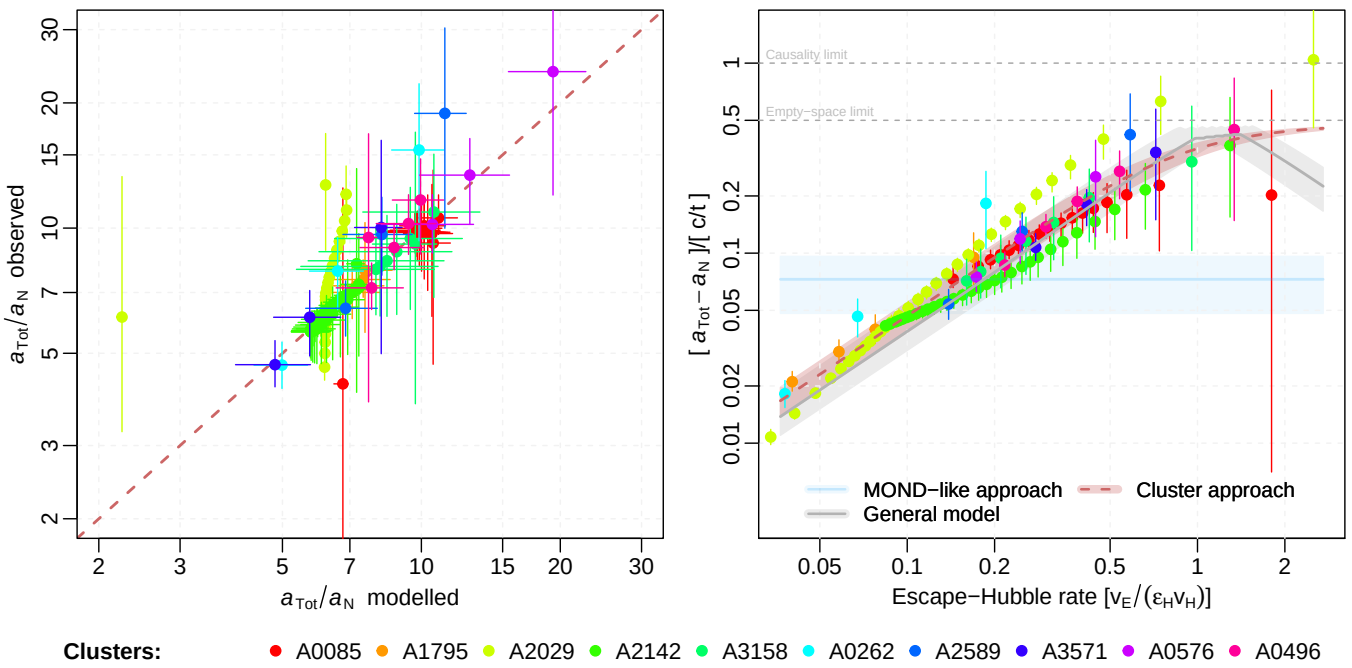

Figure 1. RAR modelling with HMG for total acceleration (a_{Tot}) compared to Newtonian acceleration (a_N). *Left*: Individual fitting (Eqs. 3 and 4) for the galaxy clusters considered (Li et al. 2023) with two parameters (ε_H and γ_{galaxy}; Table 1). *Right*: Global fitting for all data according to three models: MOND-like constant (blue band), general model (gray band, Eqs. 2 and 5), and the cluster model (red band, Eqs. 2 and 4). The MOND-like model with constant $\gamma_0^{-1} = \gamma_{sys}^{-1}\cos\gamma_{sys}$ was considered with $\gamma_{sys} = 0.466^{+0.011}_{-0.01}\pi$, which corresponds to a Milgrom's constant of $a_0 = 2\gamma_0^{-1}c/t = 1.01^{+0.33}_{-0.32}\times10^{-10}\mathrm{m\,s^{-2}}$ (Monjo 2023). In the right panel, both the general model and the specific approach for clusters use only one free parameter (ε_H), by setting the projective angle of galaxies as $\gamma_{galaxy} = \pi/2$ and $\gamma_U = \pi/3$: The general model (gray band) is represented by the value of $\varepsilon_H = 56^{+22}_{-12}$, while the cluster approach (red band) considers an average of $\varepsilon_H = 40^{+8}_{-6}$. The shaded areas represent the 90% confidence interval.

compatible with the best MOND functions (Fig. 2 *top right*). It is important to note that HMG predicts the form of the interpolating function, which is arbitrary in MOND and must be found from observations.

Furthermore, after applying an observational constraint of Eq. 5 to the galaxy rotation curves with $\gamma_U = \pi/3$, a value of $\varepsilon_H = 21^{+32}_{-11}$ is obtained for $\gamma_{center} = \pi/2$, and $\varepsilon_H = 18^{+28}_{-10}$ for $\gamma_{center} = 0.48\pi$, which are statistically compatible with the cluster-based fitting of $\varepsilon_H = 56^{+22}_{-12}$ (Fig. 2 *bottom left*). In particular, a value of $\epsilon_H \approx 45$ is compatible with both datasets but with a wide variability between the different cases. However, the parameter ε_H is not free at all because a significant correlation ($R > 0.85$, p-value < 0.001) of $\varepsilon_H \propto \sqrt{\rho}$ is found for the galactic mass densities ρ at distances between 50-200 kpc (Appendix C.4, Fig. C.3), which gives $\varepsilon_H \approx \sqrt{\rho/\rho_{vac}}$ for the vacuum density $\rho_{vac} = 3/(8\pi G t^2)$. Therefore, this justifies the name of the parameter ε_H as the square root of the *relative density of the neighborhood* (Eq. C13). Finally, an empirical relationship ($R > 0.80$, p-value < 0.001) is also found between $\cos\gamma_{center}$ and $\log(\varepsilon_H)$ for galaxies, which suggests that γ_{center} strongly depends on the geometrical features of the gravitational system.

3.3. *Prediction for small systems*

For small gravitational systems, the escape velocity v_E is much higher than the Hubble flux v_H, so it is expected that the cosmic effects are negligible (with $v_E/v_H \gg \varepsilon_H$). This is because the ratio between escape speed and Hubble flux is independent of the size of a spherical system with constant density, but smaller systems are usually much denser than larger systems. For example, according to Eq. 5, an anomaly of only $6.4^{+1.0}_{-0.4}\times10^{-17}$ m/s^2 (90% confidence level) is predicted for the Solar System at a distance of the Pluton orbit (40 AU). The predicted anomaly is even smaller for Saturn at 10 AU, which is well consistent with the null detection of anomalous effects there from Cassini radio tracking data (Hees et al. 2014; Desmond et al. 2024). For the Oort cloud, which hypothetically extends between 2 and 200 kAU, the predicted anomaly $\Delta a := \gamma_0^{-1}c/t$ increases from $2.2^{+0.4}_{-0.1}\times10^{-14}$ m/s^2 to $2.3^{+0.4}_{-0.1}\times10^{-11}$ m/s^2, respectively.

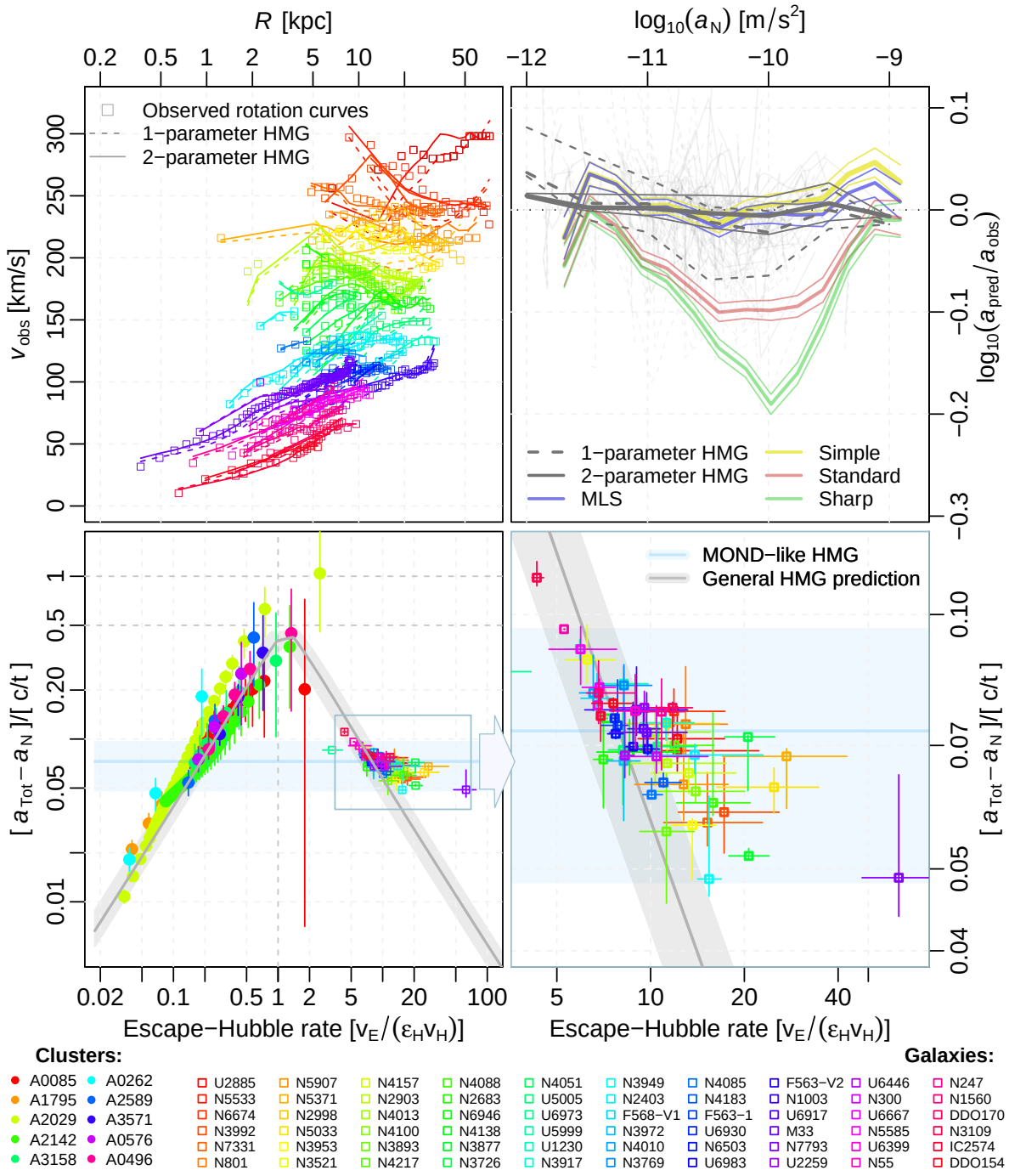

Figure 2. Galaxy rotation curves (squares, McGaugh et al. 2007) compared with cluster RAR (circles, Li et al. 2023). *Top left*: Fitting of galaxy rotation curves according to the HMG model (Eq. C26, Monjo 2023), where γ_0 is modeled by Eq. 5 with one free parameter (ϵ_H, while $\gamma_{center} = 0.48\pi$; dashed lines) or two parameters (ϵ_H, γ_{center}; continuous lines). *Top right*: Performance of the 1-parameter (dashed gray lines) and 2-parameter (continuous gray lines) model for the ratio of predicted (a_{pred}) and observed (a_{obs}) centripetal acceleration for the 60 galaxies (light gray lines) and comparison with MOND interpolation functions (MLS, simple, standard, and sharp functions, fitted to 153 suitable galaxies): 1-σ confidence intervals for all functions (upper and lower lines of each color) were found as in Fig. 23 of Banik et al. (2023). *Bottom left*: Global fitting of the dataset according to Eqs. 2 and 5. *Bottom right*: Zoom in on the theoretical prediction made for galaxies fitted with Eq. 5 with $\varepsilon_H = 21^{+32}_{-11}$. As in Fig. 1, the general model prediction for galaxies (gray band) corresponds to the parameter $\varepsilon_H = 56^{+22}_{-12}$ as an average value of the cluster fitting, with fixed $\gamma_{center} = \pi/2$ and $\gamma_U = \pi/3$. To compare, the MOND-like model and the observational constraint of the general HMG model are shown with the shaded area representing the 90% confidence interval.

The last one is about 20% of the Milgrom acceleration $a_0 \approx 1.2 \times 10^{-10}$ m/s^2 and could therefore be detected in the future. The most aligned finding is that shown by the work of Migaszewski (2023), who suggest that Milgromian gravity could explain the observed anomalies of extreme trans-Neptunian objects such as the Oort cloud (2–200 kAU, up to 20% of a_N). Brown & Mathur (2023) claimed that the farthest Kuiper Belt objects ($\sim$ 250 AU) also present a MOND signal, but the orbit integrations performed by Vokrouhlický et al. (2024) suggest that this interpretation neglects the crucial role of the external field direction rotating as the Sun orbits the Galaxy. Therefore, these findings require further analysis to compare them with the hypothesis of a ninth planet in the trans-Neptunian region (Batygin et al. 2024). In fact, Vokrouhlický et al. (2024) exclude the possible effects of MOND on scales up to about 5–10 kAU, which is more consistent with the findings of Migaszewski (2023).

In the case of wide binaries, the typical escape speed at $r \sim 0.1$ pc is about $v_E = 500$ m/s, while the Hubble flux is $v_H = r/t \sim 7 \times 10^{-3}$ m/s. Thus, the Newtonian acceleration is $a_N = \frac{1}{2}v_E^2/r \sim 4.1 \times 10^{-11}$ m/s^2 $< a_0 \approx 1.2 \times 10^{-10}$ m/s^2, which is theoretically within the classical MOND regime of Milgrom theory ($a_N < a_0$). However, the escape flux is $v_E/v_H = 7.1 \times 10^4$, and therefore we expect a very low anomaly (i.e., a large projective angle γ_{sys}). Assuming that $\gamma_{center} = \pi/2$, $\gamma_U = \pi/3$ and a global value $\varepsilon_H = 40^{+30}_{-20}$ in Eq. 5, the projective angle $\gamma_{sys} = \pi/2 - 2.20^{+0.14}_{-0.35} \times 10^{-4}\pi$, which corresponds to a projection parameter of $\gamma_0^{-1} = \gamma_{sys}^{-1} \cos\gamma_{sys} = 4.4^{+0.7}_{-0.3} \times 10^{-4}$, so the acceleration anomaly would be $\Delta a := a_{Tot} - a_N = \gamma_0^{-1} c/t = 3.1^{+0.4}_{-0.2} \times 10^{-13}$ m/s^2 (90% interval). The prediction corresponds to 2.8×10^{-13} m/s^2 $< \Delta a < 4.3 \times 10^{-13}$ m/s^2 at the 95% confidence level.

Therefore, in any case, the acceleration anomalies expected for rapid-escape systems are less than 1% of the original Milgrom constant $a_0 \approx 1.2 \times 10^{-10}$ m/s^2. This result is consistent with recent comparisons between standard gravity and MOND with data from Gaia wide-binary systems (Pittordis & Sutherland 2019, 2023; Banik et al. 2023). However, some authors dispute these results by using different data selection criteria (see, for instance, Hernandez 2023; Hernandez et al. 2023; Chae 2023, 2024a,b).

4. CONCLUDING REMARKS

Acceleration is not a geometrical invariant, but depends on the reference system or framework considered. The hyperconical model showed that it is possible to derive local-scale general relativity (that is, HMG) to model gravitational systems with anomalous acceleration similar to that attributed to dark matter or dark energy (Monjo & Campoamor-Stursberg 2023; Monjo 2023).Other MOND-based relativistic theories also obtained good performance when modeling galaxy rotation curves with a single global parameter based on acceleration. However, parameters other than acceleration are required, given that the classical MOND-based RAR does not extend to clusters and that gravity is mostly Newtonian on scales smaller than about 10 kAU with high precision, even at low acceleration.

This paper presented a generalized applicability of the HMG model for a wide range of acceleration anomalies in gravitational systems. Good agreement was obtained with the data collected from 10 galaxy clusters and 60 high-quality galaxy rotation curves. The technique developed for the perturbed metric follows the geometric definition of the sinus of a characteristic angle γ_{sys} as a function of the escape speed (v_E) and the Hubble flux ($\epsilon_H v_H$), that is, $\sin\gamma_{sys}^2 - \sin^2\gamma_U \approx \beta^2(r)\left|v_E^2 - \epsilon_H^2 v_H^2(r)\right|$ for $\gamma_U = \pi/3$. The function $\beta(r)$ does not depend on the speeds, but can be avoided by setting two parameters in $\gamma_{sys} = \gamma_{sys}(\gamma_{center}, \varepsilon_H)$: a central projective angle $0.47\pi \lesssim \gamma_{center} \lesssim 0.50\pi$ and a relative density $\varepsilon_H \geq 1$.

From the fitting of the general model of γ_{sys} (Eq. 5) to the cluster RAR data, an anomaly between $0.05\,c/t$ and $0.40\,c/t$ is predicted for the galaxy rotation dynamics, which is statistically compatible with the observations of $0.07^{+0.03}_{-0.02}c/t$. As for any modified gravity, the challenge was to derive a tight RAR compatible with observations with few free parameters. Classical MOND only has a global free parameter a_0, but does not specify the interpolating function, so MOND actually has a high freedom to fit the observations of galactic dynamics. In contrast, the HMG model derives a unique interpolation function for rotation curves using only two parameters ($\varepsilon_H, \gamma_{center}$) that are not totally free, since they are related to the density of matter.

For objects of the outer Solar System such as the farthest Kuiper Belt objects or the Oort cloud, anomalies between 10^{-14} m/s^2 and 10^{-11} m/s^2 are predicted at 1 kAU and at 100 kAU, respectively. Similarly, for wide binary systems, anomalies are expected within the range of $2.8 \times 10^{-13} < \Delta a < 4.3 \times 10^{-13}$ m/s^2 (95% confidence level). Such small predicted anomalies imply that local wide binaries should be Newtonian to high precision, as is within the observational limits. This work provides a chance to falsify a wide range of predictions of a relativistic MOND-like theory that has previously collected successful results in cosmology (Monjo 2024a). In future work, we will address

other open challenges, such as the modeling of cosmic structure growth and dynamics as well as the evolution of early stages of the universe.

ACKNOWLEDGEMENTS

IB is supported by Science and Technology Facilities Council grant ST/V000861/1. The authors thank Prof. Stacy McGaugh for providing the data for 60 high-quality galaxy rotation curves. The data set corresponding to the 10 galaxy clusters was provided by Prof. Pengfei Li, so we greatly appreciate this kind gesture.

DATA AVAILABILITY

In this study, no new data was created or measured.

APPENDIX

A. PERTURBED VACUUM LAGRANGIAN DENSITY

This appendix summarizes the definition of the local Einstein field equations according to the hyperconical model, that is, by assuming that GR is only valid at local scales (Monjo & Campoamor-Stursberg 2020; Monjo 2024a). In particular, the new Lagrangian density of the Einstein-Hilbert action is obtained by extracting the background scalar curvature R_{hyp} from the total curvature scalar $R \to \Delta R := R - R_{hyp}$ as follows:

$$\mathcal{L} = \frac{1}{16\pi G}\Delta R + \mathcal{L}_M \;=\; \frac{1}{16\pi G}\left(R + \frac{6}{t^2}\right) - \rho_M \;=\; \frac{c^2}{16\pi G}R - \Delta\rho\,, \tag{A1}$$

where G is the Newtonian constant of gravitation, $R_{hyp} = -6/t^2$ is the curvature scalar of the (empty) hyperconical universe, $\mathcal{L}_M = -\rho_M$ is the Lagrangian density of classical matter, and $\Delta\rho := \rho_M - \rho_{vac}$ is the density perturbation compared to the 'vacuum energy' $\rho_{vac} = 3/(8\pi G t^2)$ with mass-related event radius $r_M := 2G\widetilde{M} := 2G\rho_{vac}\,\frac{4}{3}\pi t^3 = t$, where $\widetilde{M}$ is a 'total mass' linked to ρ_{vac}. Moreover, the squared escape velocity associated with ρ_{vac} at r is $v_E^2(\rho_{vac}) = 2G\rho_{vac}\,\frac{4}{3}\pi r^3 = r^2/t^2 = v_H^2$. Therefore, a total density ρ_M leads to a total (classical) squared escape velocity $v_E^2(\rho_M)$ as follows:

$$v_E^2(\rho_M) = 2G\rho_M\,\frac{4}{3}\pi r^3 = 2G\left(\rho_{vac} + \Delta\rho\right)\frac{4}{3}\pi r^3 = \frac{r^2}{t^2} + \frac{2GM}{r} = v_E^2(\rho_{vac}) + v_E^2(\Delta\rho)\,, \tag{A2}$$

where we use the definition of $M := \Delta\rho\,\frac{4}{3}\pi r^3$. Now, let $\theta_M := M/\widetilde{M} \ll 1$ be a (small) constant fraction of energy corresponding to the perturbation $\Delta\rho$, and $r_M := 2GM = \theta_M t$ be the radius of the mass-related event horizon. Thus,

$$\frac{2GM}{r} = \frac{\theta_M t}{r'\frac{t}{t_0}} = \frac{\theta_M t_0}{r'} =: \frac{2GM_0}{r'}\,. \tag{A3}$$

Therefore, the quotient $M/r = M_0/r'$ is as comoving as $r/t = r'/t_0$.

Moreover, the background metric of the universe has a Ricci tensor with components $R^u_{00} = 0$ and $R^u_{ij} = \frac{1}{3}R_u\,g_{ij}$ (Monjo 2017; Monjo & Campoamor-Stursberg 2020). Since $R_{hyp} = -6/t^2$, the Einstein field equations become locally converted to (Monjo 2024a):

$$\begin{cases} \kappa P_{00} & = \Delta R_{00} - \frac{1}{2}\Delta R g_{00} \;=\; R_{00} - \frac{1}{2}R g_{00} - \frac{3}{t^2}g_{00} \\ \kappa P_{ij} & = \Delta R_{ij} - \frac{1}{2}\Delta R g_{ij} \;=\; R_{ij} - \frac{1}{2}R g_{ij} - \frac{1}{t^2}g_{ij} \end{cases}, \tag{A4}$$

where $\kappa = 8\pi G$ and $P_{\mu\nu}$ are the stress-energy tensor components. Notice that, for small variations in time $\Delta t = t - t_0 \ll t_0 := 1$, the last terms ($3/t^2$ and $1/t^2$) are equivalent to consider a 'cosmological (almost) constant' or dark energy with equation of state $w = -1/3$ (varying as a^{-2}).

B. HYPERCONICAL MODIFIED GRAVITY (HMG)

B.1. *Hyperconical universe and its projection*

This appendix reviews the main features of relativistic MOND-like modified gravity derived from the hyperconical model and referred to here as HMG (Monjo 2017, 2018; Monjo & Campoamor-Stursberg 2020, 2023; Monjo 2023). Let $\mathcal{H}^4$ be a (hyperconical) manifold with the following metric:

$$ds^2_{hyp} \approx dt^2\left(1-kr'^2\right) - \frac{t^2}{t_0^2}\left(\frac{dr'^2}{1-kr'^2} + r'^2 d\Sigma^2\right) - \frac{2r't}{t_0^2}\frac{dr'dt}{\sqrt{1-kr'^2}}\,, \tag{B5}$$

where $k = 1/t_0^2$ is the spatial curvature for the current value $t_0 \equiv 1$ of the age t of the universe, while $\frac{a}{(}t) := t/t_0$ is a scale factor, $r' \ll t_0$ is the comoving , and Σ represents the angular coordinates. Both the (Ricci) curvature scalar and the Friedmann equations derived for $k = 1$ are locally equivalent to those obtained for a spatially flat ($K_{FLRW} = 0$) ΛCDM model with linear expansion (Monjo & Campoamor-Stursberg 2020). In particular, the local curvature scalar at every point ($r' \equiv 0$) is equal to (Monjo 2017):

$$R_{hyp} = -\frac{6}{t^2} = R_{FLRW}\Big|_{K=0,\ a=t/t_0}\,, \tag{B6}$$

as for a three-sphere (of radius t). This is not accidental because, according to Monjo & Campoamor-Stursberg (2020), the local conservative condition in dynamical systems only ensures internal consistency for $k = 1$.

The hyperconical metric (Eq. B5) has shift and lapse terms that produce an apparent radial inhomogeneity, which is equivalent to an acceleration. This inhomogeneity can be assimilated as an apparent acceleration by applying some 'flattening' or spatial projection. In particular, for small regions, a final intrinsic comoving distance $\hat{r}'$ can be defined by an α-distorting stereographic projection (Monjo 2018; Monjo & Campoamor-Stursberg 2023),

$$r' \mapsto \hat{r}' = \frac{r'}{\left(1-\frac{\gamma(r')}{\gamma_0}\right)^{\alpha}}\,, \tag{B7}$$

$$t \mapsto \hat{t} = \frac{t}{1-\frac{\gamma(r')}{\gamma_0}}\,, \tag{B8}$$

where $\gamma = \gamma(r') := \sin^{-1}(r'/t_0)$ is the angular comoving coordinate, $\gamma_0^{-1} \in (0,1)$ is a projection factor, and $\alpha = 1/2$ is a distortion parameter, which is fixed according to symplectic symmetries (Monjo & Campoamor-Stursberg 2023). Locally, for empty spacetimes, it is expected that $\gamma_0 \approx 2$; which is compatible with the fitted value of $\gamma_0 = 1.6^{+0.4}_{-0.2}$ when Type Ia SNe observations are used (Monjo & Campoamor-Stursberg 2023). In summary, the projection factor γ_0 depends on a projective angle γ_{sys} such that $\gamma_0 = \gamma_{sys}/\cos(\gamma_{sys}) \geq 1$, where $\gamma_0 = 2$ corresponds to a total empty projective angle of $\gamma_{sys} \approx \pi/3$, and $\gamma_0 = 1$ is the minimum projection angle allowed by the causality relationship of the arc length $\gamma_0 t_0$. Therefore, the projective angle for an empty or almost empty neighborhood is approximately $\gamma_{neigh} = (0.284 \pm 0.049)\pi \lesssim \pi/3 =: \gamma_U$.

B.2. *Perturbation by gravitationally bound systems*

In the case of an (unperturbed) homogeneous universe, the linear expansion of $\mathcal{H}^4$ can be expressed in terms of the vacuum energy density $\rho_{vac}(t) = 3/(8\pi G t^2)$, where G is the Newtonian gravitational constant, and thus $\rho_{vac}(t_0) = \rho_{crit}$. That is, one can define an inactive (vacuum) mass or energy $\mathcal{M}(r) = \rho_{vac}\frac{4}{3}\pi r^3$ for a distance equal to r with respect to the *reference frame origin*. Using the relationship between the original coordinates $(dt, dr, r\,d\Sigma)$ and the comoving ones $(dt, \frac{a}{(}t)\,dr', \frac{a}{(}t)r'd\Sigma)$, the spatial dependence of the metric is now

$$\frac{r'^2}{t_0^2} = \frac{r^2}{t^2} = \frac{2G\rho_{vac}\frac{4}{3}\pi r^3}{r} = \frac{2G\mathcal{M}(r)}{r} = v_H^2(r)\,, \tag{B9}$$

where $v_H(r) := r/t$ is the Hubble speed, which coincides with the escape speed of the empty spacetime with vacuum density ρ_{vac}.

Definition B.1 (Mass of perturbation) *A perturbation of the vacuum density $\rho_{vac} \to \rho_M(r) := \rho_{vac} + \Delta\rho$, with an effective density $\Delta\rho$ at $r > 0$, leads to a system mass $M_{sys} := \frac{4}{3}\pi r^3 \Delta\rho$ that is likewise obtained by perturbing the curvature term,*

$$\frac{r^2}{t^2} \to \frac{r^2}{t_{sys}(r)^2} := \frac{r^2}{t^2} + \frac{2GM_{sys}}{r} = v_H^2(r) + v_E^2(r)\,, \tag{B10}$$

with a radius of curvature $t_{sys}(r) \in (2GM_{sys}, t]$, where $v_E(r) := \sqrt{2GM_{sys}/r}$ is the classical escape speed (Eq. A2).

An approximation to the Schwarzschild solution can be obtained in a flat five-dimensional ambient space from the hyperconical metric. For example, let $(t, \vec{r}, u) := (t, x, y, z, u) \in \mathbb{R}^{1,4}_\eta$ be Cartesian coordinates, including an extra spatial dimension u in the five-dimensional Minkowski plane. As used in hyperconical embedding, $u := t\cos\gamma - t$ is chosen to mix space and time. Now, it includes a gravity field with system mass M_{sys} integrated over a distance $\hat{r}$ such that $\sin^2\gamma := \frac{r^2}{t^2} \mapsto \frac{\hat{r}^2}{t^2} + \frac{2GM_{sys}}{\hat{r}}$. Notice that r is a coordinate related to the position considered, in contrast to the observed radial distance $\hat{r}$ or its comoving distance $\hat{r}' := (t_0/t)\hat{r}$. With this, first-order components $\hat{g}_{\mu\nu}$ of the metric perturbed by the mass are:

$$\begin{aligned}
\hat{g}_{tt} &= 2\cos\gamma - 1 \;\approx\; 1 - \frac{\hat{r}^2}{t^2} - \frac{2GM_{sys}}{\hat{r}}\,,\\
\hat{g}_{r'r'} &= -\frac{t^2}{t_0^2}\frac{1}{\cos^2\gamma} \;=\; -\frac{t^2}{t_0^2}\left(1 - \frac{\hat{r}^2}{t^2} - \frac{2GM_{sys}}{\hat{r}}\right)^{-1} \approx -\frac{t^2}{t_0^2}\left(1 + \frac{\hat{r}^2}{t^2} + \frac{2GM_{sys}}{\hat{r}}\right)\,,\\
\hat{g}_{r't} &= \frac{t}{t_0}\tan\gamma \;=\; \frac{t}{t_0}\frac{\hat{r}}{t}\left(1 - \frac{\hat{r}^2}{t^2} - \frac{2GM_{sys}}{\hat{r}}\right)^{-1/2} \approx \frac{t}{t_0}\frac{\hat{r}}{t} + O\left(\frac{\hat{r}^3}{2t^3}\right)\,,\\
\hat{g}_{\theta\theta} &= -\frac{t^2}{t_0^2}\hat{r}'^2\,,\\
\hat{g}_{\varphi\varphi} &= -\frac{t^2}{t_0^2}\hat{r}'^2\sin^2\theta\,,
\end{aligned}$$

where the hyperconical model is recovered taking $M_{sys} = 0$. Therefore, assuming linearized perturbations of the metric $\hat{g}_{\mu\nu} = \hat{g}^{back}_{\mu\nu} + \hat{h}_{\mu\nu}$ with $\hat{g}^{back}_{\mu\nu} := \hat{g}_{\mu\nu}|_{M_{sys}=0}$, we can find a local approach to the Schwarzschild metric perturbation $h|_{Schw}$ as follows (Monjo 2023):

$$\begin{aligned}
\hat{g}_{Schw} &:\approx \left[\eta_{\mu\nu} + \left(\hat{g}_{\mu\nu} - \hat{g}^{back}_{\mu\nu}\right)\right] dx^\mu dx^\nu \approx\\
&\approx \left(1 - \frac{2GM_{sys}}{\hat{r}}\right) d\hat{t}^2 - \frac{t^2}{t_0^2}\left[\left(1 + \frac{2GM_{sys}}{\hat{r}}\right) d\hat{r}'^2 + \hat{r}'^2 d\Sigma^2\right] + \text{shift}\,,
\end{aligned} \tag{B11}$$

which is also obtained for $\hat{g}_{\mu\nu}$ when $\hat{r}/t \ll 1$, that is $\lim_{(\hat{r}/t_0)\to 0}[\hat{g}_{\mu\nu}] \approx \hat{g}_{Schw}$. The shift term is neglected in comparison to the other terms, especially for geodesics. Our result is aligned to the Schwarzschild-like metric obtained by Mitra (2014) for FLRW metrics, specifically for the case of $K = 0$.

In summary, the first-order approach of the 5-dimensionally embedded (4-dimensional) hyperconical metric (Eq. B11) differs from the Schwarzschild vacuum solution by the scale factor t^2/t_0^2 and by a negligible shift term. Therefore, the classical Newtonian limit of GR is also recovered in the hyperconical model, because the largest contribution to gravitational dynamics is given by the temporal component of the metric perturbation h_{tt}. That is, the Schwarzschild geodesics are linearized by

$$\frac{d^2x^\mu}{d\tau^2} \approx \frac{1}{2}\eta^{\mu\nu}\frac{\partial}{\partial x^\nu}h_{tt}\left(\frac{dt}{d\tau}\right)^2\,, \tag{B12}$$

where $\hat{h}_{tt} \approx -2GM_{sys}/\hat{r}$.

C. MODELING RADIAL ACCELERATION

C.1. *Projective angles of the gravitational system*

The last appendix derived a general expression for the anomalous RAR expected for any gravitational system according to the projective angles (which depend on the quotient between escape speed and Hubble flux) under the hyperconical universe framework.

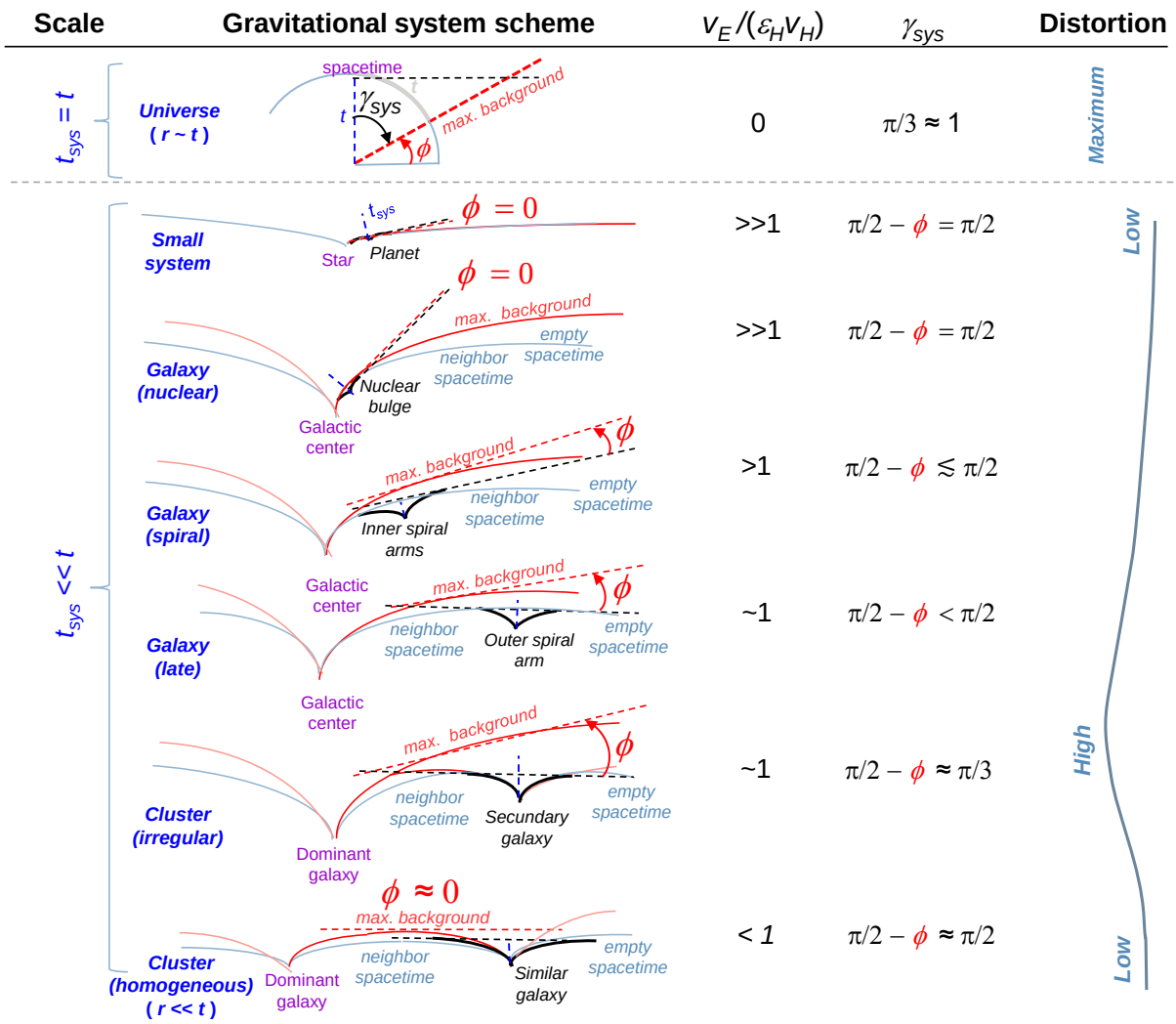

Figure C.1. Conceptual model of the projective angle γ_{sys} as a function of the relative geometry (escape speed v_E over the Hubble flux $\varepsilon_H v_H$), for each gravitational system (black curves), with respect to the maximum background spacetime (red curves). To simplify the scheme, the projection factor $\gamma_0^{-1} := \gamma_{sys}^{-1} \cos\gamma_{sys}$ is graphically represented by an auxiliary angle ϕ defined as the arc between the hyperplane of the gravitational system (dashed black line) and the maximum background hyperplane (dashed red line) curved by the dominant system (purple), such that $\gamma_{sys} = \pi/2 - \phi$. The distance scale r is represented by t_{sys} (Eq. B10). In addition to the cosmic scale, six gravitational systems are considered: i) a small system (e.g. Solar System); ii) an early-type galaxy with a dominant nuclear bulge; iii) a typical spiral galaxy; iv) a late-type spiral galaxy; v) an irregular cluster; and vi) a homogeneous cluster. The dominant objects (purple terms) are the star for a small system, the galactic center for galaxies, and the brightest galaxy for a given cluster.

From the analysis of perturbations (Eq. B10), it is expected that any gravitational system (Eq. B11) results in a characteristic scale $r_{cs}(M_{sys}(r)) := t_{sys}(r) \sin\gamma_{sys}(r)$ given by a projective angle $\gamma_{sys} \in [\pi/3, \pi/2)$ that slightly depends on the radial distance r and on the mass M_{sys}. Unlike gravitational lensing, a non-null cosmic projection $\gamma_0^{-1} = \gamma_{sys}^{-1} \cos\gamma_{sys} > 0$ is expected for non-concentrated gravitational systems. In particular, we assume that the maximum projective angle ($\gamma_{sys} = \gamma_{center} := \pi/2$, minimum cosmic projection) is produced by small, dense, and homogeneous gravitational systems, while the minimum angle ($\gamma_{sys} = \gamma_U := \pi/3$, maximum cosmic projection) corresponds to large systems extended towards an (almost) empty universe (Fig. C.1). Since $t_{sys}^2(r) \in (4G^2M_{sys}^2, t^2]$ and $r_{cs}^2(M) \in (4G^2M_{sys}^2, \frac{3}{4}t^2]$, the characteristic scale $r_{cs}^2(M_{sys})$ increases from $r_{cs}^2(M_{sys}) = t_{sys}^2(r) = 4G^2M_{sys}^2 \ll t^2$ up to $r_{cs}^2(M_{sys}) = \frac{3}{4}t_{sys}^2(r) = \frac{3}{4}t^2 = t^2 \sin^2\gamma_U$; that is, $\sin\gamma_{sys}^2(r) \in [\frac{3}{4}, 1]$.

The relation of γ_{sys} with respect to the gravitational mass and the scale of speeds can be estimated from the following properties. According to Eq. B10, a gravitational system perturbs the cosmological geometry with (squared) escape speed of $v_E^2(r) := \frac{2GM_{sys}}{r}$ higher than the Hubble expansion speed $v_H^2(r) := \frac{r^2}{t^2}$, so the projective angle γ_{sys} is given by:

$$\sin^2\gamma_{sys}(r) = \frac{r_{cs}^2(M_{sys})}{t_{sys}^2(r)} = \frac{r_{cs}^2(M_{sys})}{t^2} + \frac{2r_{cs}^2(M_{sys})\,GM_{sys}}{r^3} = \\ \approx \sin^2\gamma_{neigh} + \beta^2(r)v_E^2 \sim \sin^2\gamma_U - \beta^2(r)\epsilon_H^2 v_H^2(r) + \beta^2(r)v_E^2\,, \tag{C13}$$

where $\beta^2(r) := r_{cs}^2/r^2 \gg 1$ is an auxiliary function, $\gamma_{neigh} := \sin^{-1}(r_{cs}/t) \in (0, \gamma_U)$ is a characteristic *neighbor angle*, and $\epsilon_H^2 := \sin^2\gamma_U/\sin^2\gamma_{neigh} - 5/6 \propto t^2/r_{cs}^2 \propto \rho/\rho_{vac}$ is a *relative density* of the neighborhood matter (ρ) with respect to the vacuum density (ρ_{vac}; Eq. A2). So, roughly speaking, it is $\sin^2\gamma_{neigh}(r) \sim \frac{5}{6}\sin^2\gamma_{neigh}(r) = \sin^2\gamma_U - \epsilon_H^2 r_{cs}^2/t^2$. On the other hand, the center of the gravitational system presents a higher density, thus the cosmic projection should be minimum due to the maximum projective angle $\gamma_{center} \approx \pi/2$, that is,

$$1 \approx \sin^2\gamma_{center} \approx \frac{r_{cs}^2(M_{sys})}{t_{sys}^2(r)} + 2\epsilon_H^2\frac{r_{cs}^2(M_{sys})}{t^2} \sim \sin^2\gamma_U + \beta^2(r)\epsilon_H^2 v_H^2 + \beta^2(r)v_E^2\,. \tag{C14}$$

Notice that, for the limit when $\gamma_{neigh} \approx \gamma_U$, it is required that $\epsilon_H^2 \approx \frac{1}{6}$ and $v_E \approx 0$. The dependency of γ_{sys} on the auxiliary function $\beta(r)$ can be removed by taking the quotient of $\sin^2\gamma_{sys}(r) - \sin^2\gamma_U$ (Eq. C13) over $\sin^2\gamma_{center} - \sin^2\gamma_U$ (Eq. C13). Therefore, it is expected that the projective angle γ_{sys} of every gravitational system presents a **general relation** similar to

$$\frac{\sin^2\gamma_{sys}(r) - \sin^2\gamma_U}{\sin^2\gamma_{center} - \sin^2\gamma_U} \sim \left|\frac{v_E^2(r) - \epsilon_H^2 v_H^2(r)}{v_E^2(r) + \epsilon_H^2 v_H^2(r)}\right|, \tag{C15}$$

with two free parameters, $\epsilon_H \geq \frac{1}{6}$ and $\gamma_{center} \approx \frac{1}{2}\pi$. For example, for galaxies and small gravitational systems, the escape speed v_E^2 is strongly related to the Kepler orbital speed $v_K^2 \approx v_E^2/2 \sim v_E^2$, and the projective angle $\gamma_{sys}(r) \equiv \gamma_{galaxy}(r)$ can be estimated by the following **galactic relation** (Monjo 2023):

$$\frac{\sin^2\gamma_{galaxy}(r) - \sin^2\gamma_{neigh}}{\sin^2\gamma_{center} - \sin^2\gamma_U} \sim \frac{v_E^2(r)}{\epsilon_H^2 v_H^2(r) + v_E^2(r)}\,, \tag{C16}$$

with $\gamma_{neigh} \sim \gamma_U \approx \pi/3$ and one free parameter, which is $\epsilon_H^2 \gtrsim 1$ if $\gamma_{center} = \pi/2$ is fixed, or $\gamma_{center} \lesssim \pi/2$ if $\epsilon_H = 1$ is fixed. Thus, two limiting cases are $\sin\gamma_{sys} \approx 1 \Rightarrow \gamma_{sys} \approx \pi/2$ when orbital speed is $v_K(r) \sim v_E(r) \gg \varepsilon_H v_H(r)$, while $\sin\gamma_{sys} \approx \frac{\sqrt{3}}{2} \Rightarrow \gamma_{sys} \approx \pi/3$ when orbital speed is $v_K(r) \sim v_E(r) \ll \varepsilon_H v_H(r)$, which is the lower limit of the neighborhood projective angle (γ_{neigh}).

On the other hand, radial accelerations (without regular orbits) of large-scale objects such as galaxy clusters are expected to present opposite behavior with respect to Eq. C16, since the gravitational center is not a galactic black hole but is close to a dominant galaxy (the brightest cluster galaxies, BCGs; Shi et al. 2023; De Propris et al. 2020), and the neighborhood now corresponds to the large-scale environment of the clusters themselves. Therefore, the projective angle $\gamma_{cluster}$ of the largest structures is approximated by the following **cluster relation**:

$$\frac{\sin^2\gamma_{galaxy} - \sin^2\gamma_{cluster}(r)}{\sin^2\gamma_{galaxy} - \sin^2\gamma_U} \sim \frac{v_E^2(r)}{\epsilon_H^2 v_H^2(r) + v_E^2(r)}\,, \tag{C17}$$

where $v_E^2(r)$ is the escape speed of the clusters, $\gamma_{center} \sim \gamma_{galaxy} \lesssim \pi/2$ is the averaged projective angle for galaxies and, now, we expect that the projective angle for clusters is a variable $\gamma_{cluster}(r) \in [\pi/3, \pi/2)$, but close to the neighborhood value $\gamma_{neigh} \sim \gamma_U = \pi/3$.

However, a perfectly homogeneous distribution of low-density galaxies in a cluster will lead to a balance between the different galaxies that form it, so the cluster radial acceleration will be approximately zero ($v_E \sim 0$) and anomalies are not expected, thus the projective angle will be $\gamma_{cluster} \approx \pi/2$ for both Eq. C15 and Eq. C17; that is, no significant geometrical differences are expected between the external and internal parts of the cluster (see the last case of Fig. C.1). Conversely, for irregular clusters ($v_E \sim \epsilon_H v_H$ with $\epsilon_H \gg 1$ in Eq. C15 or $v_E^2 \gtrsim \epsilon_H^2 v_H^2(r)$ in Eq. C17), the radial acceleration will be very similar to the cosmic expansion (with angle $\gamma_{cluster} = \gamma_U = \pi/3$). Notice that, for very inhomogeneous systems ($v_E \gg \epsilon_H v_H$), Eq. C15 recovers the behavior of high-density galaxies (Eq. C16) with $\gamma_{cluster}(r) = \gamma_{galaxy}(r)$. Moreover, for $v_E \in (0,\ \epsilon_H v_H)$, Eq. C15 behaves in a similar way as in Eq. C17 as expected.

C.2. *Cosmological projection of the Schwarzschild metric*

Henceforth, the constant of light speed $c \equiv 1$ will not be omitted from the equations so we can compare with real observations later. Let λ be the scaling factor of an α-distorting stereographic projection (Eq. B7) of the coordinates $(r', u) = (ct\sin\gamma,\ ct\cos\gamma) \in \mathbb{R}^2$, used to simplify the spatial coordinates $(\vec{r}', u) \in \mathbb{R}^4$ due to angular symmetry. For nonempty matter densities, we contend that γ_{sys} depends on the escape speed of the gravity system considered. However, the first-order projection can be performed by assuming that the dependence on distances is weak (i.e., with $\gamma_0^{-1} = \gamma_{sys}^{-1}\cos\gamma_{sys}$ being approximately constant for each case). Thus, the stereographic projection is given by the scale factor λ such as (see for instance Monjo & Campoamor-Stursberg 2023; Monjo 2023):

$$\lambda = \frac{1}{1-\frac{\gamma}{\gamma_0}} \approx 1 + \frac{r'}{\gamma_0 t_0 c}\,, \tag{C18}$$

where $\gamma = \sin^{-1}[r'/(t_0 c)] \approx r'/(t_0 c)$ is the angular position of the comoving distance $r' = (t_0/t)\, r$. Therefore, the projected coordinates are

$$\begin{cases} \hat{r}' = \lambda^\alpha r' \approx \left(1 + \frac{\alpha r'}{\gamma_0 t_0 c}\right) r\,, \\ \hat{t} = \lambda t \approx \left(1 + \frac{r'}{\gamma_0 t_0 c}\right) t\,, \end{cases} \tag{C19}$$

At a local scale, the value of $\alpha = 1/2$ is required to guarantee consistency in dynamical systems (Monjo & Campoamor-Stursberg 2023), but the parameter α is not essential in this work, since only the temporal coordinate is used in our approach below.

Applying this projection to the perturbed metric (Eq. B11) and obtaining the corresponding geodesics, it is easy to find a first-order approach of the cosmic contribution to modify the Newtonian dynamics in the classical limit, as shown below (Sec. C.3).

C.3. *First-order perturbed geodesics*

Assuming that the projection factor $\gamma_0^{-1} = \gamma_{sys}^{-1}\cos\gamma_{sys}$ is approximately constant, the quadratic form of the projected time coordinate (Eq. C19) is as follows:

$$d\hat{t}^2 \approx \left(1 + \frac{2r'}{\gamma_0 t_0 c} + \frac{2t\dot{r}'}{\gamma_0 t_0 c}\right) dt^2 \quad + \quad \text{higher-order terms}\,. \tag{C20}$$

By using these prescriptions, our Schwarzschild metric (Eq. B11) is expressed in projected coordinates $(\hat{t}, \hat{r}')$ or in terms of the original ones (t, r'); that is, $\hat{g}_{Schw} = \hat{g}_{\mu\nu} d\hat{x}^\mu d\hat{x}^\nu = g_{\mu\nu} dx^\mu dx^\nu$, with

$$\hat{g}_{Schw} \approx \left(1 - \frac{2GM_{sys}}{c^2 \hat{r}}\right) c^2 d\hat{t}^2 - \frac{\hat{t}^2}{t_0^2}\,\hat{r}'^2 d\Sigma^2 \quad \approx \quad g_{tt} c^2 dt^2 + g_{ii}(dx^i)^2\,,$$

and finally, it is locally expanded up to first-order perturbations in terms of γ_0. Notice that, according to Eq. B11, the background terms r'^2/t_0^2 do not produce gravitational effects and thus they can be neglected. Here, one identifies a projected perturbation h_{tt} of the temporal component of the metric, $g_{tt} = \eta_{tt} + h_{tt} = 1 + h_{tt}$, with $\eta_{\mu\nu} = \eta^{\mu\nu} = \mathrm{diag}(1, -1, -1, -1)$. Thus, if M_{sys} is assumed to be mostly concentrated in the central region of the gravitional system, the first-order perturbation of the temporal component of the metric is

$$h_{tt} \approx -\frac{2GM_{sys}}{rc^2}\left(1 - \frac{\alpha r}{\gamma_0 tc}\right) + \frac{2}{\gamma_0 c}\left(\frac{r}{t} + \frac{t}{t_0}\dot{r}'\right)\,, \tag{C21}$$

where the spatial projection $\hat{r} \approx (1 + \alpha r/(\gamma_0 ct))\, r$ is considered (from Eq. C19), and the relation between comoving distance r' and spatial coordinate r is also used $(r'/t_0 = r/t)$.

Under the Newtonian limit of GR, the largest contribution to gravity dynamics is given by the temporal component of the metric perturbation h_{tt}. That is, Schwarzschild geodesics (Eq. B12) produce both time-like and space-like acceleration components from the metric perturbation h_{tt},

$$\frac{d^2\hat{s}}{c^2 dt^2} \approx \frac{1}{2}\frac{\partial}{\partial x^0} h_{tt}\, e_t \ - \ \frac{1}{2}\frac{\partial}{\partial x^i} h_{tt}\, e_i =: a^t e_t + a^i e_i\,, \tag{C22}$$

where the four-position $\hat{s} := (c\Delta t, x^i) = c\Delta t\, e_t + x^i\, e_i =: c\Delta \mathbf{t} + \mathbf{x} \in \mathbf{R}^{1,3}$ is assumed, with canonical basis $\{e_t, e_1, e_2, e_3\}$ and dual basis $\{e^t, e^1, e^2, e^3\}$. For a freely falling particle with central-mass reference coordinates $\mathbf{x} = x^i e_i = (r, 0, 0) = \mathbf{r} \in \mathbb{R}^3$, it experiences an acceleration of about

$$\frac{d^2\hat{s}}{dt^2} = a^t e_t + a^r e_r \approx \left(\frac{\dot{r}'}{t_0} - \frac{r + \frac{1}{2}\alpha r_M}{\gamma_0 t^2}\right) e_t \; - \; \left(\frac{GM_{sys}}{r^2} + \frac{c}{\gamma_0 t}\right)\frac{\mathbf{r}}{r} \; \approx \; a_N - \frac{c}{\gamma_0 t}\frac{\mathbf{r}}{r} - \frac{r}{\gamma_0 t^2} e_t \,, \tag{C23}$$

where $r_M := 2GM_{sys}/c^2 \ll r$ is the Schwarzschild radius, which is neglected compared to the spatial position r. That is, an acceleration anomaly is obtained mainly in the spatial direction, about $|\mathbf{a} - a_N| \approx \gamma_0^{-1} c/t$ for $\mathbf{a} := a^r e_r$. However, the total acceleration also has a time-like component, that is, in the direction e_t. In particular, for a circular orbit with radius r, and taking into account the non-zero temporal contribution to the acceleration in the hyperconical universe with radius ct (Monjo 2023), the total centrifugal acceleration is

$$\frac{v^2}{c^2} e_s = -\left(cte_t e^t + x^i e_i e^i\right)\frac{d^2\hat{s}}{c^2 dt^2} \approx ct\left(\frac{r}{\gamma_0 c^2 t^2}\right) e_t \; + \; \left(\frac{GM_{sys}}{c^2 r^2} + \frac{1}{\gamma_0 ct}\right)\frac{x^i x_i}{r}\, e_i \,, \tag{C24}$$

where e_s is an effective space-like direction ($||e_s||^2 = e_s e^s = -1$), while the absolute value of the velocity is given by

$$\frac{v^4}{c^4} = -\left|\left|\frac{v^2}{c^2} e_s\right|\right|^2 \approx \left(\frac{GM_{sys}}{rc^2}\right)^2 + \frac{2GM_{sys}}{\gamma_0 tc^3} \Longrightarrow \begin{cases} v \approx \sqrt{\frac{GM_{sys}}{r}} & \text{if } \frac{GM_{sys}}{r^2} >> \frac{2c}{\gamma_0 t} =: a_{\gamma 0} \\ v \approx \sqrt[4]{\frac{2GM_{sys}c}{\gamma_0 t}} & \text{if } \frac{GM_{sys}}{r^2} << \frac{2c}{\gamma_0 t} = a_{\gamma 0} \end{cases} , \tag{C25}$$

which satisfies two well-known limits of Newton's dynamics and Milgrom's (Eq. C25 right), where a_0 is the Milogrom's acceleration parameter and $M_{sys} = M_{sys}(r)$ is the total mass within the central sphere of radius r. Finally, the velocity curve $v = v(r)$ can be reworded in terms of the Kepler speed $v_K := \sqrt{GM_{sys}(r)/r}$. Therefore, the predicted mass-discrepancy acceleration relation for rotation curves is

$$\left(\frac{v}{v_K}\right)^2 \approx \sqrt{1 + \frac{1}{|a_N|}\frac{2c}{\gamma_0 t}} \;\; \Longrightarrow \;\; \frac{a_C}{a_N} \approx \sqrt{1 + \frac{1}{|a_N|}\frac{2c}{\gamma_0 t}} \,, \tag{C26}$$

where $a_C = v^2/r$ is the total radial acceleration and $a_N = GM_{sys}/r^2$ is the Newtonian acceleration. However, the absence of rotation in galaxy clusters leads to a radial acceleration similar to Eq. C23. In any case, the projection factor $\gamma_0^{-1} = \gamma_{sys}^{-1} \cos\gamma_{sys}$ depends on the projective angle γ_{sys}, which can be estimated from the galaxy cluster approach (Eq. C17) or from the general model (Eq. C15), respectively, as follows:

$$\sin^2\gamma_{cluster}(r) \;\; \approx \;\; \sin^2\gamma_{galaxy} - \left(\sin^2\gamma_{galaxy} - \sin^2\gamma_U\right)\frac{v_E^2(r)}{\varepsilon_H^2 v_H^2(r) + v_E^2(r)} \,, \tag{C27}$$

$$\sin^2\gamma_{cluster}(r) \;\; \approx \;\; \sin^2\gamma_U + \left(\sin^2\gamma_{center} - \sin^2\gamma_U\right)\left|\frac{v_E^2(r) - \epsilon_H^2 v_H^2(r)}{v_E^2(r) + \epsilon_H^2 v_H^2(r)}\right| . \tag{C28}$$

where γ_{center} can be fixed to $\gamma_{center} = \pi/2$ to test the 1-parameter (ϵ_H) general model of Eq. C28, while this study assumes that $\{\epsilon_H, \gamma_{galaxy}\}$ are free in our 2-parameter model for clusters (Eq. C28). Finally, the empty projective angle is usually set as $\gamma_U = \pi/3$ (Monjo & Campoamor-Stursberg 2023), which produces a projection factor of $\gamma_U^{-1}\cos\gamma_U \approx \frac{1}{2}$.

C.4. *Individual fitting*

Observed data on the RAR of 10 clusters ($0.0328 < z < 0.0899$) were collected from the study performed by Li et al. (2023). Individually, fitting of Eq. C27 for the anomaly between the total spatial acceleration and Newtonian acceleration (Eq. C23) leads to a square root of the relative density of about $\varepsilon_H = 38^{+29}_{-11}$ (90% confidence level, Fig. C.2). All these results are obtained by fixing the constants $\gamma_U = \pi/3$ and $\gamma_{center} = \pi/2$. The general model (Eq. C28), with only one free parameter (ε_H), gave good results for eight of the ten clusters, showing difficulties in fitting the more available data from the A2029 and A2142 clusters (Table 1). If two parameters are considered (ε_H, γ_{center}), the results considerably improve except for the A2029 cluster, which requires changing $\gamma_U^{-1}\cos\gamma_U \to 1$ to be compatibly fitted to the observations.

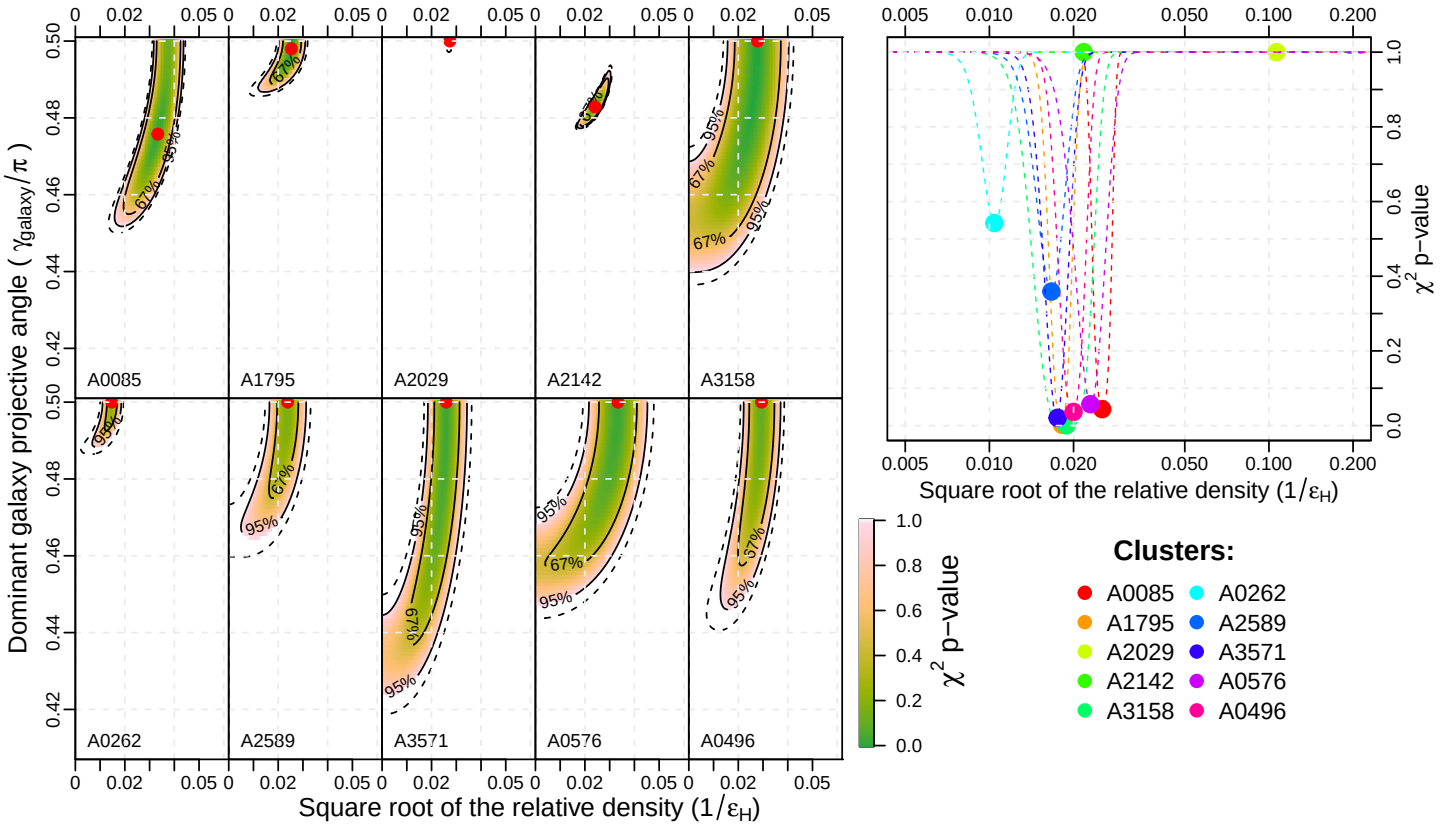

Figure C.2. Observational constraint of the proposed models fitted to RAR of the ten galaxy clusters considered (Li et al. 2023). *Left*: Best values (red points) and uncertainty area (green shaded regions: 1-σ confidence level) of the two parameters (ε_H and γ_{galaxy}, Table 1) used in fits to individual clusters according to the specific approach (Eq. C27 in C23). *Right*: Best fits of the single free parameter (ε_H) used in the general model (Eq. C28 in C23), defined for $\gamma_{center} = 0.48\pi$. In both cases (1 or 2 free parameters), the *projective angle of the neighborhood* (γ_U) was fixed to $\gamma_U = \pi/3$. Notice that cluster A2029 did not pass the chi-square test even with the 2-parameter model. However, it passed the test for $\gamma_U = 0.235\pi$, corresponding to $\gamma_U^{-1}\cos\gamma_U \approx 1$.

The same 2-parameter (ε_H, γ_{center}) general model (Eq. C28 with $\gamma_U = \pi/3$) was also applied to the 60 high-quality galaxy rotation curves, obtaining an acceptable result for all of them. The case of 1 parameter (ε_H free when $\gamma_{center} = 0.48\pi$ is set) showed a slightly larger chi-square statistic and p-value, but these are also acceptable for all of them. Moreover, an empirical relationship is found between the single parameter ϵ_H and the square root of a relative density, which defines an identity $\rho(r_{typ})/\rho_{vac} \cong 1$ in units of vacuum density $\rho_{vac} := 3/(8\pi G t^2)$ for an observed density $\rho(r_{typ})$ that is defined at a *typical neighborhood* distance of approximately four times the maximum radius ($r_{typ} \approx 4 \times r_{max}$, fitted at $R = 0.85$, p-value < 0.0001, Fig. C.3 *left*) for each galaxy rotation curve, and equal to the minimum radius ($r_{typ} \approx r_{min}$) for the data of each cluster. This *typical distance* corresponds to $r_{typ} \approx 50 - 200\,\mathrm{kpc}$.

Finally, when the 2-parameter HMG model is considered for galaxies, an additional relationship is found between ϵ_H and γ_{center}:

$$\cos(\gamma_{center}) = \cos\left(0.4610^{+0.0013}_{-0.0014}\pi\right) - (0.020 \pm 0.002)\ln(\varepsilon_H) \qquad \text{(C29)}$$

for $1 \leq \varepsilon_H < 400$, with a Pearson coefficient of $R = 0.80$ (p-value < 0.0001, Fig. C.3 *right*).

Table 1. Individual fitting of Eq. 4 to each cluster according to the general model (Eq. 5) with one parameter (ε_H), and with the specific model for clusters (Eq. 4 with two parameters, ε_H and γ_{galaxy}). The p-values is that of a lower χ^2.

Name (data)	General model		Specific model for clusters		
	ε_H	χ^2 p-value	ε_H	γ_{galaxy}/π	χ^2 p-value
A0085 (17)	40^{+6}_{-5}	0.04	31^{+5}_{-4}	$0.474^{+0.017}_{-0.009}$	< 0.01
A1795 (4)	55^{+14}_{-9}	< 0.01	39^{+6}_{-4}	$0.499^{+0.001}_{-0.006}$	< 0.01
A2029 (32)	52^{+40}_{-20}	> 0.95	37^{+15}_{-10}	$0.500^{+0}_{-0.002}$	> 0.95
A2142 (31)	46^{+15}_{-15}	> 0.95	41^{+4}_{-2}	$0.483^{+0.003}_{-0.002}$	< 0.01
A3158 (7)	53^{+39}_{-17}	< 0.01	37^{+18}_{-8}	$0.491^{+0.009}_{-0.030}$	< 0.01
A0262 (3)	96^{+32}_{-19}	0.54	67^{+10}_{-6}	$0.500^{+0}_{-0.005}$	0.57
A2589 (3)	60^{+37}_{-14}	0.36	41^{+10}_{-4}	$0.500^{+0}_{-0.013}$	0.47
A3571 (3)	57^{+22}_{-12}	0.02	39^{+8}_{-6}	$0.495^{+0.005}_{-0.036}$	0.14
A0576 (3)	44^{+22}_{-11}	0.06	31^{+8}_{-6}	$0.493^{+0.007}_{-0.023}$	0.13
A0496 (5)	50^{+16}_{-9}	0.04	33^{+6}_{-4}	$0.500^{+0}_{-0.028}$	0.14

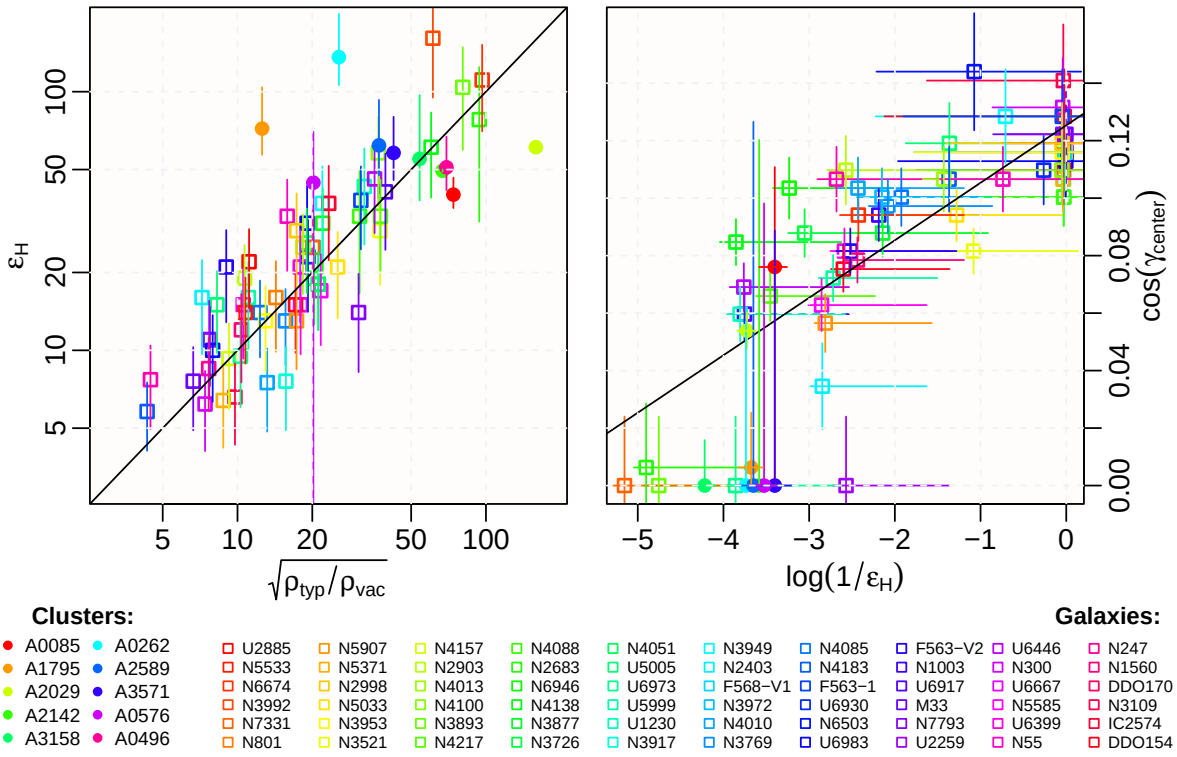

Figure C.3. Model parameters fitted to the 60 high-quality galaxy rotation curves (squares), empirical relationships (black lines), and comparison with the fitting to the RAR data of 10 clusters (circles). *Left*: Constraint of the 1-parameter HMG model (when $\gamma_{center} = 0.48\pi$ is set, while ε_H is free) for galaxies, which shows an empirical identity between the single parameter ϵ_H and the square root of a relative density ρ_{typ}/ρ_{vac}. That is, in units of vacuum density $\rho_{vac} := 3/(8\pi G t^2)$, an observed density $\rho_{typ} := \rho(r_{typ})$ is defined at a typical distance of $r_{typ} \sim 50 - 200$ kpc, whose fit has been found ($R = 0.85$, p-value < 0.0001) as four times the maximum radius ($r_{typ} \approx 4 \times r_{max}$) for each galaxy rotation curve, and equal to the minimum radius ($r_{typ} \approx r_{min}$) for the data of each cluster. *Right*: Constraint on the 2-parameter HMG model for galaxies, which shows a relationship between ϵ_H and γ_{center} according to $\cos(\gamma_{center}) = \cos(0.460\pi) - 0.020\ln(\varepsilon_H)$ for $1 \leq \varepsilon_H < 400$, with a Pearson coefficient of $R = 0.80$ (p-value < 0.0001; black regression line).

REFERENCES

Aalbers, J., Akerib, D. S., Akerlof, C. W., et al. 2023, PhRv. Lett., 131, 041002. https://link.aps.org/doi/10.1103/PhysRevLett.131.041002

Abel, C., Ayres, N. J., Ban, G., et al. 2017, Physical Review X, 7, 041034

Ardi, E., & Baumgardt, H. 2020, JPCS, 1503, 012023. https://dx.doi.org/10.1088/1742-6596/1503/1/012023

Asencio, E., Banik, I., Mieske, S., et al. 2022, MNRAS, 515, 2981. https://doi.org/10.1093/mnras/stac1765

Banik, I., Pittordis, C., Sutherland, W., et al. 2023, MNRAS, 527, 4573. https://doi.org/10.1093/mnras/stad3393

Banik, I., & Zhao, H. 2022, Symmetry, 14, doi:10.3390/sym14071331. https://www.mdpi.com/2073-8994/14/7/1331

Barkana, R. 2018, Nature, 555, 71. https://doi.org/10.1038/nature25791

Batygin, K., Morbidelli, A., Brown, M. E., & Nesvorný, D. 2024, ApJL, 966, L8

Bekenstein, J. D. 2004, PhRvD, 70, 083509. https://link.aps.org/doi/10.1103/PhysRevD.70.083509

Blanchet, L. 2007, CQGra, 24, 3529. https://dx.doi.org/10.1088/0264-9381/24/14/001

Blanchet, L., & Skordis, C. 2024, ArXiv e-prints, Arxiv, arXiv:2404.06584

Brown, K., & Mathur, H. 2023, AJ, 166, 168. https://dx.doi.org/10.3847/1538-3881/acef1e

Cattaneo, A., Salucci, P., & Papastergis, E. 2014, ApJ, 783, 66. https://dx.doi.org/10.1088/0004-637X/783/2/66

Chae, K.-H. 2022, ApJ, 941, 55. https://dx.doi.org/10.3847/1538-4357/ac93fc

—. 2023, ApJ, 952, 128. https://dx.doi.org/10.3847/1538-4357/ace101

—. 2024a, arxiv, doi:10.48550/arXiv.2309.10404. https://doi.org/10.48550/arXiv.2309.10404

—. 2024b, arxiv, doi:10.48550/2402.05720. https://doi.org/10.48550/arXiv.2402.05720

Chae, K.-H., Lelli, F., Desmond, H., et al. 2020, ApJ, 904, 51. https://dx.doi.org/10.3847/1538-4357/abbb96

Ciufolini, I., Matzner, R., Paolozzi, A., et al. 2019, Scientific Reports, 9, 15881

Comerón, S., Trujillo, I., Cappellari, M., et al. 2023, A&A, 675, A143. https://doi.org/10.1051/0004-6361/202346291

de Blok, W. J. G., Walter, F., Brinks, E., et al. 2008, AJ, 136, 2648. https://dx.doi.org/10.1088/0004-6256/136/6/2648

De Propris, R., West, M. J., Andrade-Santos, F., et al. 2020, MNRAS, 500, 310. https://doi.org/10.1093/mnras/staa3286

Desmond, H. 2016, MNRAS, 464, 4160. https://doi.org/10.1093/mnras/stw2571

Desmond, H., Hees, A., & Famaey, B. 2024, MNRAS, 530, 1781. https://doi.org/10.1093/mnras/stae955

Di Cintio, A., & Lelli, F. 2015, MNRAS Lett., 456, L127. https://doi.org/10.1093/mnrasl/slv185

Dittus, H., & Lämmerzahl, C. 2007, AdSpR, 39, 244. https://www.sciencedirect.com/science/article/pii/S0273117707001858

Du, P., Egana-Ugrinovic, D., Essig, R., & Sholapurkar, M. 2022, PhRvX, 12, 011009. https://link.aps.org/doi/10.1103/PhysRevX.12.011009

Eckert, D., Ettori, S., Pointecouteau, E., van der Burg, R. F. J., & Loubser, S. I. 2022, A&A, 662, A123. https://doi.org/10.1051/0004-6361/202142507

Famaey, B., & McGaugh, S. S. 2012, LiRvRe, 15, 10. https://doi.org/10.12942/lrr-2012-10

Goddy, J. S., Stark, D. V., Masters, K. L., et al. 2023, MNRAS, 520, 3895. https://doi.org/10.1093/mnras/stad298

Harikumar, S., & Biesiada, M. 2022, EuPhJC, 82, 241. https://doi.org/10.1140/epjc/s10052-022-10204-4

Haslbauer, M., Banik, I., & Kroupa, P. 2020, MNRAS, 499, 2845. https://doi.org/10.1093/mnras/staa2348

Hees, A., Folkner, W. M., Jacobson, R. A., & Park, R. S. 2014, PhRvD, 89, 102002. https://link.aps.org/doi/10.1103/PhysRevD.89.102002

Hernandez, X. 2023, MNRAS, 525, 1401. https://doi.org/10.1093/mnras/stad2306

Hernandez, X., Verteletskyi, V., Nasser, L., & Aguayo-Ortiz, A. 2023, MNRAS, 528, 4720. https://doi.org/10.1093/mnras/stad3446

Hoof, S., Geringer-Sameth, A., & Trotta, R. 2020, JCAP, 2020, 012. https://dx.doi.org/10.1088/1475-7516/2020/02/012

Hu, X.-S., Zhu, B.-Y., Liu, T.-C., & Liang, Y.-F. 2024, PhRvD, 109, 063036. https://link.aps.org/doi/10.1103/PhysRevD.109.063036

Katz, A., Reece, M., & Sajjad, A. 2016, PDU, 12, 24. https://www.sciencedirect.com/science/article/pii/S2212686416000042

Keenan, R. C., Barger, A. J., & Cowie, L. L. 2013, ApJ, 775, 62. https://dx.doi.org/10.1088/0004-637X/775/1/62

Kroupa, P. 2015, CJP, 93, 169. https://doi.org/10.1139/cjp-2014-0179

Kroupa, P., Gjergo, E., Asencio, E., et al. 2023, PoS Corfu2022, 436, arXiv:2309.11552. https://doi.org/10.22323/1.436.0231

Leauthaud, A., Finoguenov, A., Kneib, J.-P., et al. 2010, ApJ, 709, 97. https://dx.doi.org/10.1088/0004-637X/709/1/97

Lelli, F., McGaugh, S. S., & Schombert, J. M. 2016, ApJ, 152, 157. https://dx.doi.org/10.3847/0004-6256/152/6/157

Lelli, F., McGaugh, S. S., Schombert, J. M., Desmond, H., & Katz, H. 2019, MNRAS, 484, 3267. https://doi.org/10.1093/mnras/stz205

Lelli, F., McGaugh, S. S., Schombert, J. M., & Pawlowski, M. S. 2017, ApJ, 836, 152. https://dx.doi.org/10.3847/1538-4357/836/2/152

Li, P., Tian, Yong, Júlio, Mariana P., et al. 2023, A&A, 677, A24. https://doi.org/10.1051/0004-6361/202346431

Liu, X.-H., Li, Z.-H., Qi, J.-Z., & Zhang, X. 2022, ApJ, 927, 28. https://dx.doi.org/10.3847/1538-4357/ac4c3b

Mavromatos, N. E., Sakellariadou, M., & Yusaf, M. F. 2009, PhRvD, 79, 081301. https://link.aps.org/doi/10.1103/PhysRevD.79.081301

Mazurenko, S., Banik, I., Kroupa, P., & Haslbauer, M. 2023, MNRAS, 527, 4388. https://doi.org/10.1093/mnras/stad3357

McGaugh, S. S. 2004, ApJ, 609, 652. https://dx.doi.org/10.1086/421338

McGaugh, S. S., de Blok, W. J. G., Schombert, J. M., de Naray, R. K., & Kim, J. H. 2007, ApJ, 659, 149. https://dx.doi.org/10.1086/511807

McGaugh, S. S., Lelli, F., & Schombert, J. M. 2016, PhRvL, 117, 201101. https://link.aps.org/doi/10.1103/PhysRevLett.117.201101

Merritt, D. 2017, Stud. Hist. Philos. Sci. B Stud. Hist. Philos. Modern Phys., 57, 41. https://www.sciencedirect.com/science/article/pii/S1355219816301563

Migaszewski, C. 2023, Monthly Notices of the Royal Astronomical Society, 525, 805. https://doi.org/10.1093/mnras/stad2250

Milgrom, M. 1983, ApJ, 270, 365

Mitra, A. 2014, MNRAS, 442, 382. https://doi.org/10.1093/mnras/stu859

Moffat, J. W., & Toth, V. T. 2009, MNRAS, 397, 1885. https://doi.org/10.1111/j.1365-2966.2009.14876.x

—. 2013, Galaxies, 1, 65. https://www.mdpi.com/2075-4434/1/1/65

Monjo, R. 2017, PhRvD, 96, 103505. https://link.aps.org/doi/10.1103/PhysRevD.96.103505

—. 2018, PhRvD, 98, 043508. https://link.aps.org/doi/10.1103/PhysRevD.98.043508

—. 2023, CQGra, 40, 235002. https://iopscience.iop.org/article/10.1088/1361-6382/ad0422

—. 2024a, ApJ, 967, 66. https://dx.doi.org/10.3847/1538-4357/ad3df7

—. 2024b, Phd thesis, Complutense University of Madrid, Madrid, Spain, https://10.5281/zenodo.11001487

Monjo, R., & Campoamor-Stursberg, R. 2020, CQGra, 37, 205015. https://dx.doi.org/10.1088/1361-6382/abadaf

—. 2023, CQGra. http://iopscience.iop.org/article/10.1088/1361-6382/aceacc

Pittordis, C., & Sutherland, W. 2019, MNRAS, 488, 4740. https://doi.org/10.1093/mnras/stz1898

—. 2023, OJAp, 6, doi:10.21105/astro.2205.02846

Roshan, M., Ghafourian, N., Kashfi, T., et al. 2021, MNRAS, 508, 926. https://doi.org/10.1093/mnras/stab2553

Seifert, M. D. 2007, PhRvD, 76, 064002. https://link.aps.org/doi/10.1103/PhysRevD.76.064002

Shi, D., Wang, X., Zheng, X., et al. 2023, arxiv:astro-ph.GA, arXiv.2303.09726, doi:10.48550/arXiv.2303.09726. https://doi.org/10.48550/arXiv.2303.09726

Skordis, C., & Złośnik, T. 2021, Phys. Rev. Lett., 127, 161302. https://link.aps.org/doi/10.1103/PhysRevLett.127.161302

Stiskalek, R., & Desmond, H. 2023, Monthly Notices of the Royal Astronomical Society, 525, 6130. https://doi.org/10.1093/mnras/stad2675

Tian, Y., Ko, C.-M., Li, P., McGaugh, S., & Poblete, S. L. 2024, A&A, 684, A180

Tian, Y., Umetsu, K., Ko, C.-M., Donahue, M., & Chiu, I.-N. 2020, ApJ, 896, 70. https://dx.doi.org/10.3847/1538-4357/ab8e3d

Touboul, P., Métris, G., Rodrigues, M., et al. 2022, CQGra, 39, 204009. https://dx.doi.org/10.1088/1361-6382/ac84be

Trippe, S. 2014, Zeitschrift Naturforschung Teil A, 69, 173

Vokrouhlický, D., Nesvorný, D., & Tremaine, S. 2024, ApJ, in press, arXiv:2403.09555